Transactions of the SMiRT 27
Yokohama, Japan, March 3-8, 2024
Division VII

DEVELOPMENT OF FAILURE MITIGATION TECHNOLOGIES FOR IMPROVING RESILIENCE OF NUCLEAR STRUCTURES (3) FAILURE MITIGATION OF REACTOR VESSELS FOR EXCESSIVE EARTHQUAKES

Yiji YE[1], Sho Hasegawa[2], Masakazu Ichimiya[2], Naoto Kasahara[2]

[1] PhD Student, The University of Tokyo, Tokyo, Japan (ye-yiji@g.ecc.u-tokyo.ac.jp)
[2] The University of Tokyo, Tokyo, Japan

ABSTRACT

During excessive earthquakes, the Fast Reactor Main Vessel (FRMV) is vulnerable to buckling because of its thin-walled cylindrical structure. Buckling deformation should not be considered as a limit state in BDBEs. Instead, the objective is to achieve a stable post-buckling state. In the present study, the post-buckling behaviour of pool-type FRMV is experimentally studied, where two kinds of thin-walled cylindrical models are subjected to intense horizontal vibration to cause buckling. Regardless of buckling configuration, the frequency ratio becomes higher than one after buckling, which prevents the post-buckling response from divergence even intense acceleration continues to input. The comparison among different buckling configurations confirms that a higher H/R ratio shows better resilience against catastrophic collapse after buckling than that a low H/R ratio in terms of response reduction. This is attributed to significantly different degradation behaviour of structural stiffness.

INTRODUCTION

As a lesson learned from the Fukushima nuclear power plant accident, the nuclear industry recognized the importance of mitigating accident consequences after Beyond Design Basis Events (BDBEs), which would lead to terrible consequences despite a low likelihood of occurrence (Kasahara et al., 2020). BDBEs usually occur due to extreme conditions such as excessive seismic load. During such events, resilience to failure consequences is required for structures. Stable failure modes (e.g., plastic deformation) are allowed in this case, the safety design focuses on the prevention of unstable failure modes (e.g., fracture and collapse) and the chain failure sequences (i.e., extension from stable failure modes to unstable failure modes) (Kasahara et al., 2019). To develop mitigation approach for BDBEs, it is essential to understand the realistic failure mechanisms of the structures under extreme loading conditions.

Under excessive seismic loading, the Fast Reactor Main Vessel (FRMV) is vulnerable to buckling because of its thin-walled large-diameter cylindrical structure. In conventional structural design, buckling occurrence is usually carefully prevented for it causes immediate collapse of the entire structure, especially under load-controlled conditions. Nevertheless, seismic buckling could show significantly different characteristics because seismic loads have alternative load-controlled and displacement-controlled characteristics (Kasahara et al., 2020). Buckling deformation without causing immediate collapse should not be considered as a limit state of FRMV in BDBEs because it has minor influence on safety function. Instead, the objective is to achieve a stable state after buckling.

As a particular issue, buckling of FRMV has been widely investigated as a part of design studies of demonstration fast reactors since the last century, typically in Japan. The goal of these efforts was to prepare a design guideline against buckling occurrence of the FRMV under seismic load (Hagiwara et al., 1991; Akiyama et al., 1993). In these studies, the post-buckling behavior was evaluated by conservative method to meet the safety goal of DBEs, while it is not necessarily suitable for BDBEs, which adopt best estimation for actual failure modes. In alignment with the augmented safety requirements for BDBEs after the Fukushima nuclear accident, further studies are required for a comprehensive understanding of the post-buckling behaviour of FRMV under excessive seismic loads.

In our previous study, the post-buckling behaviour of loop-type FRMV has been experimentally investigated (Ye et al., 2023). Under excessive horizontal vibration, localized bending buckling mode is the dominant for loop-type FRMV. In this case, due to substantial degradation of structural stiffness, the post-buckling response has a frequency ratio higher than one such that response divergence is prevented. Meanwhile, the response is notably delayed from the input, which impedes the conversion of input energy into kinetic energy, reducing the inertial impact to the structure. These mechanisms ensure a global response stability after buckling.

Other than loop-type FRMV design, pool-type FRMV is also an important mainstream design concept globally. As a parallel study, the post-buckling behaviour of pool-type FRMV is evaluated in the present study. Dynamic buckling experiments are carried out, where thin-walled cylindrical models are subjected to intense horizontal vibration to cause buckling. The post-buckling behaviour is carefully scrutinized. A comparison with regards to stability after buckling is conducted among different buckling configurations.

METHODOLOGY

Experimental setup

Figure 1 shows the photo of experimental facility. A cylindrical test model hangs a set of weight plates and is suspended on a steel support constraint on the shaking table. Two side windows are intended on the side support legs to facilitate the observation on the buckling process. Under horizontal excitation provided by the shaking table, the lumped weight applies a global inertial transverse load on the lower end of the test model. This configuration simulates the realistic loading condition of FRMV subjected to a horizontal motion.

The specifications of the experimental models are given in Table 1. Key geometrical parameters of the straight cylindrical part of the pool-type FRMV designed by JAEA (Kubo et al., 2020) are also given in Table 1. Two kinds of test models are used in the experiments (short model and medium model), which diverge in the maximum bending stress-to-maximum shear stress ratio (H/R). Figure 2 shows the interaction effects between shear and bending buckling modes (Matsuura et al., 1993). It highlights that bending stress predominates with high H/R ratio and the cylinder exhibits a localized bending mode. Conversely, a low H/R ratio leads to a pure shear mode. As depicted in the figure, the H/R ratio of the pool-type FRMV is approximate to the short model.

Test conditions

Test conditions are detailed in Table 2. Sinusoidal and seismic wave are used as input accelerations. The former is ideal for fundamental mechanism study while the latter can verify the applicability of the knowledge learned from the sinusoidal input. The seismic wave is a specific segment extracted from the time history record of the 2016 Kumamoto Earthquake, notable for containing the ‘killer pulse’. This record is selected for it is characterized by a dominant region and a concentration around a predominant frequency, aiding the analysis of the response spectrum. Prior to being used as input waves, the Fourier spectrum is translated in frequency domain to align the dominant frequency with the target input frequency. The input acceleration amplitudes are chosen to exceed the threshold acceleration to induce buckling of the cylindrical model. After buckling initiation, the same input wave was applied for several times more successively to confirm the tendency of post-buckling response.

In the experiments, the relative response displacement and absolute response acceleration are measured at the location of centre of gravity of the lumped weight, respectively by laser displacement sensor and accelerometer. The input acceleration is also recorded. The initial natural frequency of the test model is measured by impulse tests. High-speed camera is used to capture the buckling initiation and post-buckling response.

Figure 1. Photograph of experimental facility

Table 1: Specifications of the experimental models and straight cylindrical part of the reactor vessel

Type		R* (mm)	L* (mm)	H* (mm)	t* (mm)	R/t (-)	H/R (-)	Material
Test model	Short	26	26	41.2	0.2	131	1.58	304 stainless steel
	Medium	26	52	67.3	0.2	131	2.58	
Straight cylindrical part of the FRMV		8595	18350	12850	50	172	1.50	316FR stainless steel

* R: inner radius; L: Length of the cylinder; H: Length of bending moment arm; t: thickness

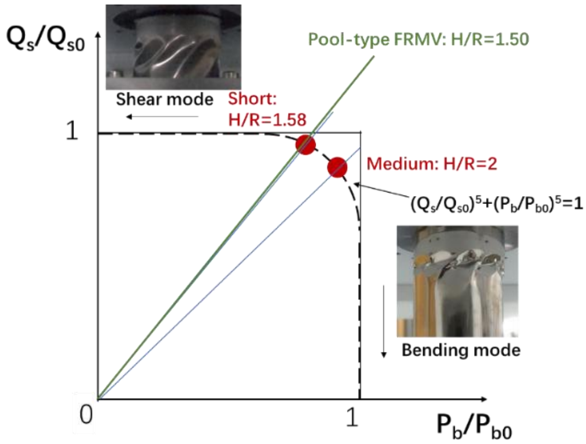

Figure 2. Interaction effects between shear and bending buckling modes (Matsuura et al., 1993)

Table 2: Test conditions

No.	Model type (-)	Initial natural frequency (Hz)	Weight (kg)	Input waveform (-)	Input frequency (Hz)	Maximum input acceleration (m/s^2)
1	Short	64	26.7	Sinusoidal	25	120
2	Short	64	26.7	Sinusoidal	50	80
3	Short	64	26.7	Seismic	25	102
4	Short	64	26.7	Seismic	50	90
5	Medium	64	26.7	Sinusoidal	18	81
6	Medium	48	26.7	Sinusoidal	35	92
7	Medium	48	26.7	Seismic	18	95
8	Medium	48	26.7	Seismic	35	85

Energy balance method

In the dynamic analysis, the test model carrying a lumped weight can be regarded as a Single Degree-Of-Freedom (SDOF) system. The classic equation of motion in relative reference system is given as

$$m\ddot{x} + c\dot{x} + f(x) = -m\ddot{x}_g \tag{1}$$

where:
x: relative response displacement of the lumped weight
c: viscous damping factor
m: lumped weight subjected to excitation
$\ddot{x}_g$: acceleration of the foundation (i.e., the steel support and shaking table)
$f(x)$: the restoring force from the test model

Or, this equation can be rewritten in the absolute reference system for a better physical description (Uang, 1990):

$$m\ddot{x}_{abs} + c\dot{x} + f(x) = 0 \tag{2}$$

where $\ddot{x}_{abs}$ is absolute response acceleration of the lumped weight

Physically, the first term $m\ddot{x}_{abs}$ on the left-hand side of Equation 2 represents the inertial load applied to the test model during vibration. It is also the same as the total force applied to the steel support. By multiplying relative response velocity of the mass $\dot{x}$ to each term, the instantaneous energy balance of the system can be obtained:

$$m\ddot{x}_{abs}\dot{x} + [c\dot{x} + f(x)]\dot{x} = 0 \tag{3}$$

$$\underbrace{m\ddot{x}_{abs}\dot{x}_{abs}}_{\dot{E}_k} + \underbrace{[c\dot{x} + f(x)]\dot{x}}_{\dot{E}_d} = \underbrace{m\ddot{x}_{abs}\dot{x}_g}_{\dot{E}_i} \tag{4}$$

where $\dot{x}_{abs}$ and $\dot{x}_g$ represent respectively the absolute response velocity of the lumped weight and the absolute velocity of the foundation. In Equation 4, the right-hand term ($\dot{E}_i$) quantifies the mechanical power exerted by the total base transverse load at the steel support level in reaction to the displacement of the steel support. This reflects the instantaneous energy input from the external source into the system. The two terms on the left-hand side of the equation, however, represent two recipients of the input energy. The first term ($\dot{E}_k$) is the instantaneous kinetic energy directly correlated with the inertial load amplitude applied to the test model and causes immediate damage. Thus, this term is considered as a destabilization factor. The second term ($\dot{E}_d$) captures the instantaneous energy dissipation mechanisms within the system including energy loss due to damping and the energy absorbed either by recoverable elastic strain energy or irrecoverable hysteretic (or plastic) strain energy. Contrary to the kinetic energy, the second recipient represents a way of progressive damage and is considered as a stabilization factor in the time scale of a general seismic input.

Equivalent linear response method

The natural frequency of the test model is an important indicator in the dynamic analysis. In the pre-buckling response, the test model is characterized by an individual natural frequency. While after buckling initiation, the response becomes nonlinear and the test model is characterized by a spectrum of frequencies. The equivalent linear response method is practically used in the present study to analyze the post-buckling response in a simplified way.

The idea is to assimilate the nonlinear response of Equation 1 into an equivalent highly-damped linear elastic system:

$$m\ddot{x} + c_{eq}\dot{x} + k_{eq}x = -m\ddot{x}_g \tag{5}$$

where c_{eq} and k_{eq} denote the equivalent viscous damping factor and equivalent linear structural stiffness. The equivalent natural frequency can be calculated as

$$f_{eq} = \frac{1}{2\pi}\sqrt{\frac{k_{eq}}{m}} \tag{6}$$

For each hysteretic cycle, the equivalent stiffness is evaluated by a least-square formula (Pegon et al., 2017):

$$k_{eq} = \frac{N\sum(x(n)P(n)) - (\sum x(n))\sum P(n)}{N\sum x(n)^2 - (\sum x(n))^2} \tag{7}$$

where:
N: total number of discrete point coordinate $(x,\ P)$ of the hysteretic cycle
n: index number of point
P: structural response to the inertial load applied by the lumped weight (i.e., $P = -m\ddot{x}_{abs}$).

The equivalent viscous damping factor is evaluated by a classic manner from the quotient of absorbed and elastic energy:

$$c_{eq} = \frac{k_{eq}}{4\pi^2 f_i}\frac{E_d}{E_{el}} \tag{8}$$

where:
f_i: frequency of the external excitation
E_d: cumulative dissipated energy in one cycle, calculated by the area enclosed by the hysteretic cycle
E_{el}: maximum elastic strain energy stored during the cycle, calculated by

$$E_{el} = \frac{k_{eq}{x_{max}}^2}{2} \tag{9}$$

with x_{max} being maximum response displacement in the cycle.

RESULTS AND DISCUSSION

Buckling modes

Figure 3 displays the process of buckling initiation and development in both short and medium models, as recorded by high-speed camera. For the short model, a pure shear mode initiated under cyclic load, characterized by alternating inclined wrinkles that extend across the entire cylinder. After several subsequent vibrations, crack initiation is observable at some intersections of these alternating wrinkles. In contrast, the medium model exhibits a bending mode priorly with a small horizontal deflection of the cylinder, which is characterized by several localized inward-bended dimples near the upper end of the cylinder. As deflection increases, alternating inclined wrinkles emerge from the bending dimples and extend towards lower end of the cylinder. Under sufficient loading cycles, crack initiation is probable either at the cusps of the dimples at the front side and back side of the cylinder or at the intersections of inclined alternating wrinkles.

Compared with pure bending mode configuration studied in our previous study, where fatigue cracks are always initiated near the upper end of the cylinder, the pure shear mode in the short model and the bending-shear mode in the medium model observed in the present study have a lower tolerance to crack initiation for it has a more severe impact on the safety function of these buckled bodies.

Post-buckling response

Figures 4 to 7 display the time history records of response displacement and acceleration for both models, under sinusoidal and seismic inputs. In both models, the initiation of buckling results in a significant increase in response displacement. However, after buckling, an immediate divergence in response is never observed, suggesting that buckling doesn’t progress even intense acceleration continues to input.

Table 3 summarizes the maximum response acceleration and displacement. After the onset of buckling, the medium model shows a decrease in maximum response acceleration with subsequent inputs, whereas in the short model, it remains relatively constant. On the other hand, the maximum response displacement amplitude remains almost constant in subsequential inputs in both models.


370 ms (Buckling initiation)


404 ms


547 ms

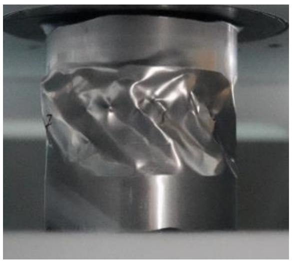
1000 ms (End)

(a) Short model (Test No.1)


70 ms (Initiation of bending mode)


280 ms (Initiation of shear mode)


352 ms


510 ms (End)

(a) Medium model (Test No.6)

Figure 3. Buckling initiation and development process in both models

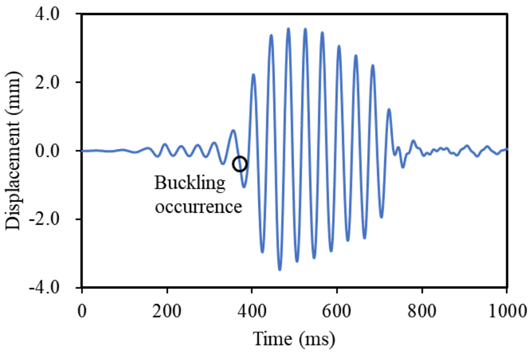

(a) Response displacement

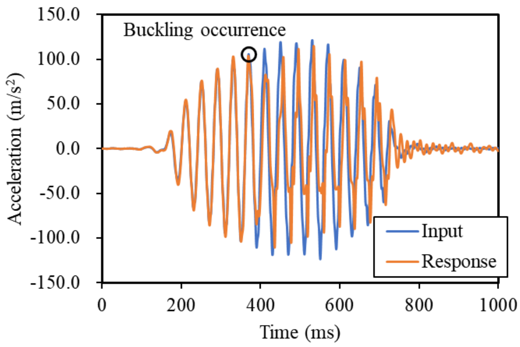

(b) Response acceleration

Figure 4. Short model: Sinusoidal wave (Test No.1)

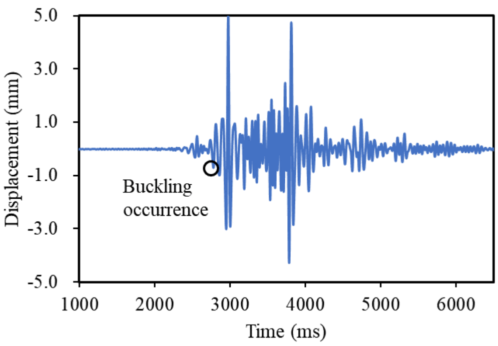

(a) Response displacement

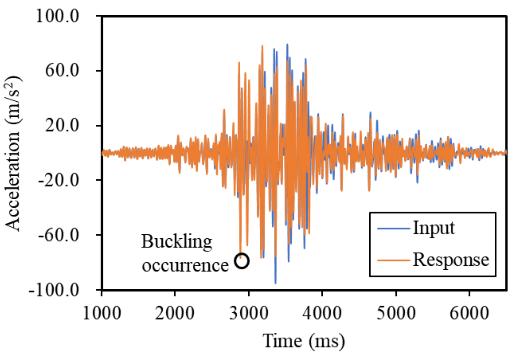

(b) Response acceleration

Figure 5. Short model: Seismic wave (Test No.3)

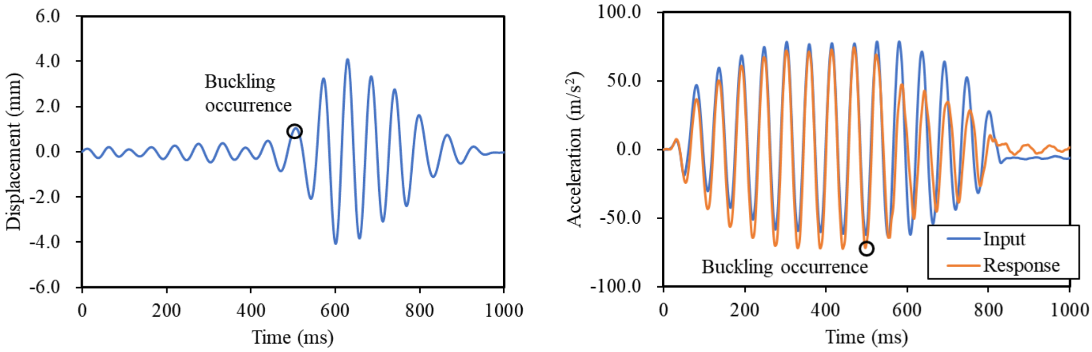

(a) Response displacement (b) Response acceleration

Figure 6. Medium model: Sinusoidal wave (Test No.5)

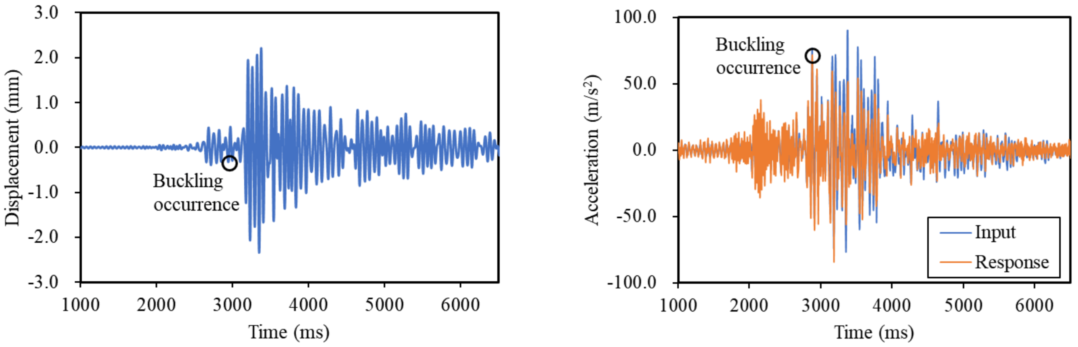

(a) Response displacement (b) Response acceleration

Figure 7. Medium model: Seismic wave (Test No.7)

Table 3: Summary of maximum response acceleration and displacement

No.	Model type (-)	Input waveform (-)	Input frequency (Hz)	Maximum input acceleration (m/s^2)	Maximum response acceleration (m/s^2)				Maximum response displacement (mm)			
					A_1*	A_2*	A_3*	A_4*	D_1*	D_2*	D_3*	D_4*
1	Short	Sinusoidal	25	130	109	108	-	-	5.5	6.4	-	-
2	Short	Sinusoidal	50	120	98	88	83	93	1.1	1.0	1.0	1.1
3	Short	Seismic	25	100	91	90	98	-	4.9	4.3	4.9	-
4	Short	Seismic	50	95	83	89	83	80	0.9	1.1	1.2	1.1
5	Medium	Sinusoidal	18	90	73	51	46	-	6.0	6.1	6.3	-
6	Medium	Sinusoidal	35	95	69	50	35	38	1.7	2.0	1.9	2.0
7	Medium	Seismic	18	95	75	61	56	55	5.7	5.8	5.9	6.1
8	Medium	Seismic	35	90	70	56	57	54	1.7	1.9	1.9	1.9

* A_n: acceleration; D_n: displacement; n: the input sequence number

The equivalent linear response method is applied to analyze post-buckling response. Table 4 provides a summary of key parameters. The initial frequency ratios R_1 and post-buckling frequency ratio R_2 are defined as

$$R_1 = \frac{f_i}{f_0} \tag{10}$$

$$R_2 = \frac{f_i}{f_{post}} \tag{11}$$

where f_0, f_{post} and f_i refer to initial natural frequency, post-buckling natural frequency and input frequency, respectively. Similar to observations in the bending buckling configuration, the increase of natural frequency is identified as the primary reason to prevent the buckled model from immediate response divergence. As illustrated in Table 4, the response shifts from R_1<1 to R_2>1 after buckling. When frequency ratio is higher than one, increasing frequency ratio leads to decease of the response, thereby weakening the diminution tendency of the structural stiffness, which in turn prevents the increase of frequency ratio. Consequently, the response of system is stabilized. It is also recognized that the post-buckling response in the short model is generally closer to the resonant peak (R_2=1) than in the medium model. These observations are valid regardless of input waveforms, indicating a validity in a general seismic scenario.

Associated with increase in natural frequency, the response becomes delayed behind the input to a certain degree. As detailed in Table 4, the post-buckling phase delay in the short model is less pronounced than in the medium model. From the perspective of energy balance, the phase delay is a limiting factor that prevent the transfer of input energy into kinetic energy. Figure 8 compares the instantaneous energy balance between short and medium model. Following the initiation of buckling, the phase delay between kinetic energy peak and input energy peak is relatively small in the short model, whereas it is sufficiently large in the medium model. Consequently, the majority of input energy is dissipated through hysteretic behaviour rather than being converted into kinetic energy in the medium model. In contrast, most of the input energy is still converted into kinetic energy in the short model.

Table 4: Summary of key parameters evaluated by equivalent linear response method

No.	Model type (-)	Input waveform (-)	$f_i{}^*$ (Hz)	$f_0{}^*$ (Hz)	$R_1{}^*$ (-)	$f_{post}{}^*$ (Hz)	$R_2{}^*$ (-)	$\xi_{eq}{}^*$ (-)	$\theta_2{}^*$ (π)
1	Short	Sinusoidal	25	64	0.39	20	1.25	0.60	0.15
2	Short	Sinusoidal	50	64	0.78	40	1.25	0.55	0.10
3	Short	Seismic	25	64	0.39	22	1.14	0.63	-
4	Short	Seismic	50	64	0.78	42	1.19	0.60	-
5	Medium	Sinusoidal	18	48	0.38	8.5	2.12	0.54	0.47
6	Medium	Sinusoidal	35	48	0.73	15	2.33	0.40	0.43
7	Medium	Seismic	18	48	0.38	10	1.80	0.50	-
8	Medium	Seismic	35	48	0.73	20	1.75	0.60	-

* f_i: input frequency; f_0: initial natural frequency; f_{post}: equivalent natural frequency after buckling; R_1, R_2: initial frequency ratio and post-buckling frequency ratio; ξ_{eq}: equivalent viscous damping factor θ_2: the phase delay of response with respects to input after buckling

Comparison among different buckling configurations

Figure 9 presents a comparison of different buckling configurations in terms of correlation between initial and post-buckling frequency ratio. They are represented by H/R ratios: H/R=6.9 (pure bending mode), H/R=2 (bending-shear mode), H/R=1.1 (pure shear mode). Experimental data of H/R=6.9 is referred to our previous study. Under constant initial frequency ratio, the post-buckling response is closer to resonance when shear mode becomes dominant (low H/R ratio) and farther from resonance when bending mode is dominant (high H/R ratio). This is attributed to significantly different degradation behaviour of structural stiffness after buckling. In the shear mode, shear-type wrinkles extend across the entire cylinder, implying a global resistance against external loads. Consequently, the declination in structural stiffness after buckling is gradual. On the contrary, bending mode is localized and the declination of structural stiffness is rapid. Consequently, the post-buckling equivalent natural frequency is higher in shear mode than bending mode.

Figure 10 illustrates the correlation between normalized applied transverse load and normalized maximum response displacement after buckling. With higher H/R ratio, the transverse load applied to the buckled cylinder tends to decrease as the maximum deflection increases. However, in the case of low H/R ratio, the applied load remains relatively rigid and almost independent of the deflection of the cylinder. Therefore, the buckled model is subjected to an increased risk of crack initiation within the time scale of an excessive earthquake. These results confirm that configuration with higher H/R ratio shows better resilience to withstand catastrophic collapse after buckling than that with low H/R ratio.

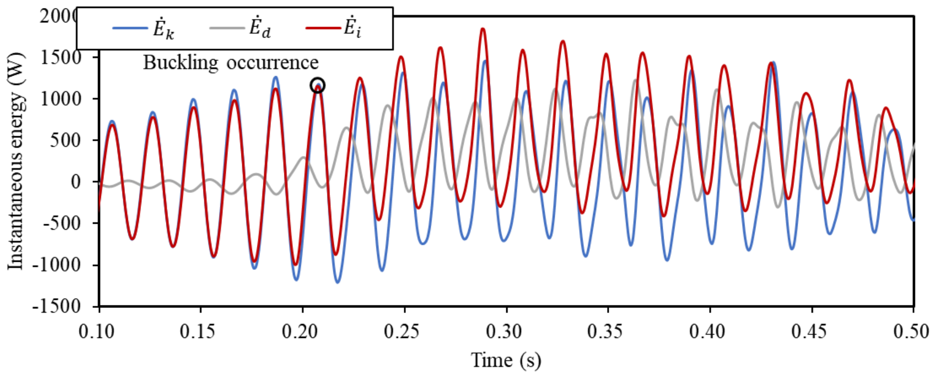

(a) Short model (Test No.1)

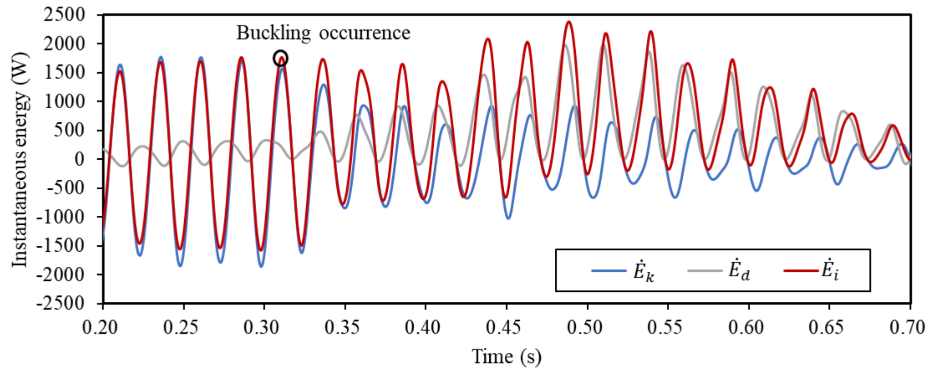

(b) Medium model (Test No.5)

Figure 8. Instantaneous energy balance evolution

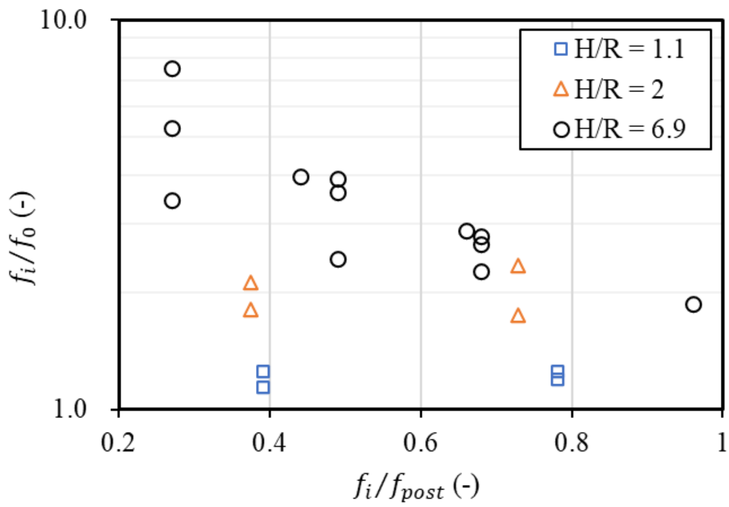

Figure 9. Initial frequency ratio vs. Post-buckling equivalent frequency ratio

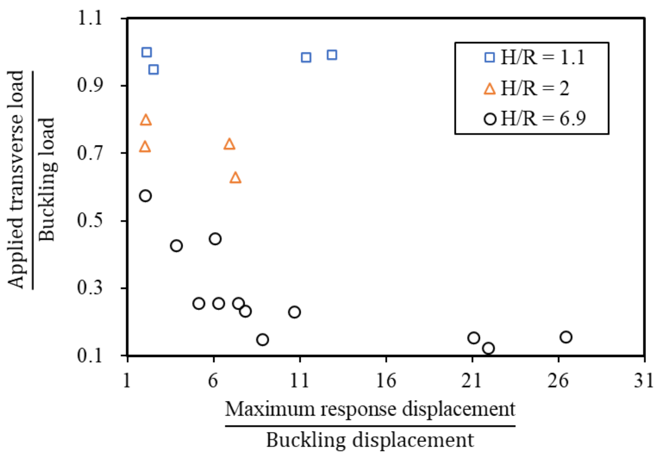

Figure 10. Normalized maximum response displacement vs. Normalized applied transverse load

CONCLUSION

In the present study, the post-buckling behaviour of pool-type FRMV is experimentally studied. Dynamic buckling experiments are carried out, where thin-walled cylindrical models are subjected to intense horizontal vibration to cause buckling. Two kinds of cylindrical models with different H/R ratios are used in the experiments, such that the pool-type FRMV design is intermediate between two configurations. The post-buckling behaviour is carefully scrutinized with regards to stability after buckling. Two major conclusions are obtained from the above discussion.

1. Due to increase of natural frequency after buckling, the frequency ratio is higher than one, which prevents the post-buckling response from divergence even intense acceleration continues to input. This finding is independent of buckling configuration.

2. Higher H/R ratio shows better resilience to withstand catastrophic collapse after buckling than low H/R ratio. As H/R ratio increases, localized bending mode becomes dominant and has rapid degradation in structural stiffness. The post-buckling response is thus farther from resonance with substantial phase delay behind input, leading to reduction of applied transverse load. In contrast, shear mode is dominant with low H/R ratio, resulting in a gradual declination of structural stiffness. Post-buckling response is closer to resonance with limited phase delay, thus no reduction in the applied load.

REFERENCES

Akiyama, H., Ohtsubo, H., Nakamura, H., et al., 1993, “Outline of the seismic buckling design guideline of an FBR-a tentative draft,” Nuclear Engineering and Design, Vol. 140(3).

Hagiwara, Y., Akiyama, H., Kokubo, K., et al., 1991, “Post-buckling behaviour during earthquakes and seismic margin of FBR main vessels”, Int. J. Press. Vessels Pip, Vol. 45(3).

Kasahara, N., Wakai, T., Nakamura, I., et al, 2019, “Research plan and progress to realize fracture control of nuclear components”, ASME PVP2019-93545.

Kasahara, N., Al Bari, M., Sakemi, R., 2020, “Failure modes of piping under seismic loads which have both load and displacement controlled characteristics”, Int. J. Press. Vessels Pip, Vol. 179.

Kubo, S., Chikazawa, Y., et al., 2020, “A conceptual design study of pool-type sodium-cooled fast reactor with enhanced anti-seismic capability,” Mechanical Engineering Journal, Vol. 7(3).

Pegon, P., Molina, F., 2017, “Least-square effective stiffness to be used with equivalent viscous damping as equivalent linear model,” Publications Office of European Union

Matsuura, S., Nakamura, H., Ogiso, S., et al., 1993, “Formulae for Evaluating Buckling Strength of FBR Main Vessels under Earthquake Loading”, JSME International Journal Series B, Vol. 36(3).

Uang, C., 1990, “Evaluation of seismic energy in structures,” Earthq. Eng. Struct. Dyn., Vol. 19.

Ye, Y., Hasegawa, S., Kasahara, N., 2023, “Study on dynamic buckling behavior and post-buckling stability of thin-walled cylinders subjected to lateral vibration,” ASME PVP2023-105543.